Lasers in Surgery and Medicine 28:56–66 (2001)

Reflectance Spectroscopy for In Vivo Characterization of Ovarian Tissue

Urs Utzinger, PhD,[1] Molly Brewer, DVM, MD, MS,[2,3] Elvio Silva, MD,[4] David Gershenson, MD,[3] Robert C. Blast, Jr., MD,[5] Michele Follen, MD, PhD,[3] and Rebecca Richards-Kortum, PhD[1]*

[1]Biomedical Engineering Program, The University of Texas at Austin, Austin, Texas 78712
[2]Department of Gynecology, The University of Texas Medical School, Houston Texas 77030
[3]Department of Gynecologic Oncology, The University of Texas M. D. Anderson Cancer Center, Houston, Texas 77030
[4]Department of Pathology, The University of Texas M. D. Anderson Cancer Center, Houston, Texas 77030
[5]Division of Medicine, The University of Texas M. D. Anderson Cancer Center, Houston, Texas 77030

Background and Objective: To explore whether reflectance spectroscopy can differentiate normal ovary, benign neoplasms, and ovarian cancer.
Study Design/Materials and Methods: Reflectance spectra (390–600 nm) were measured at three source-detector separations (SDS) in vivo at 64 sites in 16 patients undergoing oophorectomy. Parameters with largest statistical differences were identified. Based on these parameters algorithms were developed and evaluated.
Results: Promising parameters were the reflectance intensity from 540 to 580 nm (SDS, 1.1 mm), the slope of the reflectance spectrum from 490 to 520 nm (SDS, 1.1 mm), the slope from 510 to 530 nm (SDS, 2.1 mm), and the slope from 510 to 530 (SDS, 3 mm). Average sensitivity and specificity were 86 ± 6% and 79 ± 5% to separate normal ovary from benign neoplasms and cancers. Average sensitivity and specificity were 86 ± 4% and 80 ± 8% to separate ovarian cancers from benign neoplasms and normal ovary.
Conclusion: Reflectance spectroscopy should be further investigated for ovarian cancer screening. Lasers Surg. Med. 28:56–66, 2001

Key words: reflectance spectroscopy; ovarian cancer detection

INTRODUCTION

Ovarian cancer causes the highest mortality of any of the gynecologic cancers and is the second most common gynecologic malignancy [1]. Women with FIGO (International Federation of Obstetrics and Gynecology) Stage I disease, which is disease limited to the ovaries, have a 5-year survival of 80–90% [2], whereas women with FIGO Stage III or IV disease (widespread cancer) have a 5-year survival of 5–30%; thus, earlier detection of these cancers would increase the survival for women with ovarian cancer.

The ability to identify preinvasive changes, benign neoplasms, and early malignant neoplasms in a minimally invasive manner could revolutionize ovarian cancer screening, particularly in women at high risk for developing ovarian cancer. Although laparoscopy permits visualization of the ovaries and identification of grossly visible neoplastic changes, it does not allow one to distinguish microscopic changes on or beneath the ovarian surface.

Currently, 70% of all ovarian cancers are diagnosed at FIGO Stage III or IV, making survival of patients with this gynecologic cancer poor. Therapy of women with advanced ovarian cancer usually requires single or multiple surgical procedures and multiple courses of chemotherapy, resulting in significant morbidity and health care costs [2,3]. The high mortality from ovarian cancer has stimulated widespread interest in developing accurate screening for ovarian cancer, yet current screening tests including CA125 [4,5], transvaginal ultrasound [6], and pelvic examination lack acceptable sensitivity and specificity (NIH consensus 1994) [7].

CA125 is a glycoprotein found in serum that is a nonspecific marker for epithelial ovarian cancer. Elevations may precede the clinical detection of ovarian cancer. In a retrospective case-control study of 105 women who eventually developed ovarian cancer and 323 matched controls, Zurawski et al. [8] found that 50% of women who developed ovarian cancer had a CA125 level greater than 30 U/ml in serum collected within 18 months of diagnosis and that 25% of women who developed ovarian cancer had an elevated CA125 in serum collected within 60 months of diagnosis. However, specificity for CA125 as a screening tool is poor in the premenopausal population because of benign conditions such as pregnancy, endometriosis, and adenomyosis that elevate CA125 levels [9]. Although serial determinations of CA125 can improve specificity, sensitivity is still limited because only 50% of clinically detectable Stage I ovarian cancers have an elevated CA125 level.

Women at low risk for developing ovarian cancer probably do not need screening for ovarian cancer. However, identifying women who are at high risk for developing

*Correspondence to: Rebecca Richards-Kortum, PhD, Department of Electrical and Computer Engineering, The University of Texas at Austin, Austin, TX 78712.
E-mail: kortum@mail.utexas.edu
Accepted 7 June 2000

ovarian cancer by virtue of family history or genetic testing [10,11] yields a cohort of women who need effective screening. Mutations in the BRCA1 and BRCA2 genes have been strongly linked to an increased susceptibility to both breast and ovarian cancer. Women with BRCA1 mutations may have a lifetime risk of developing ovarian cancer as high as 40–65% (10); for women with BRCA2 mutations, this rate is 10% [12]. Currently, assessment and screening is offered yearly or biyearly to this group of patient by using pelvic ultrasound, CA125 assay, and pelvic examination.

In search for better methods of early diagnosis and screening, several researchers have investigated both abdominal and transvaginal ultrasound imaging [6]. Transvaginal sonography (TVS) seems most promising in postmenopausal women, because increased ovarian volume and morphologic abnormalities are predictors of malignancy, but differentiation of benign and malignant disease can be difficult [13]. DePriest and Van Nagell [14] identified 44 ovarian abnormalities in 3,220 asymptomatic postmenopausal women; surgery revealed three cancers (two stage I and one stage III) and 41 benign ovarian neoplasms. Over half of the benign neoplasm were serous cystadenomas. Although sensitivity and specificity of ultrasound have been reported as 90% or greater [14–16], positive predictive values (PPV) range from 4–10%. Poor PPV, which identifies which positive tests are actually positive, may lead to unnecessary and potentially dangerous surgical procedures.

Alternatively, techniques based on quantitative optical spectroscopy have shown promise in the detection of epithelial lesions in the colon, cervix, bladder, head and neck, esophagus, and other epithelial surfaces [17–24]. Thus, our present goal was to explore whether such methods could eventually be adapted to improve early diagnosis of ovarian neoplasia.

Several optical spectroscopy techniques have been examined for detection of epithelial neoplasms, including diffuse reflectance spectroscopy [17–22], fluorescence spectroscopy [22,23], and Raman spectroscopy [24]. In diffuse reflectance spectroscopy, light incident on the tissue front surface undergoes elastic scattering and potentially absorption. Elastic scattering is produced by inhomogeneities in the tissue refractive index. Recent results [25,26] have shown that tissue backscattering is altered as the size of the nucleus increases and the nuclear texture becomes coarser. As the separation between the illumination spot and detection spot is increased, the fraction of detected light, which has undergone single backscattering decreases [27]. Tissue absorption in the ultraviolet and visible ranges is dominated by hemoglobin, with the oxygenated and de-oxygenated forms having different absorption spectra [28]. In contrast, inelastic interactions provide information about tissue fluorophores or Raman scatterers. The potential for using diffuse reflectance spectroscopy to diagnose early ovarian cancer in a cost-effective manner seems greater than that of other spectroscopic techniques, because elastic interactions are much stronger than inelastic interactions.

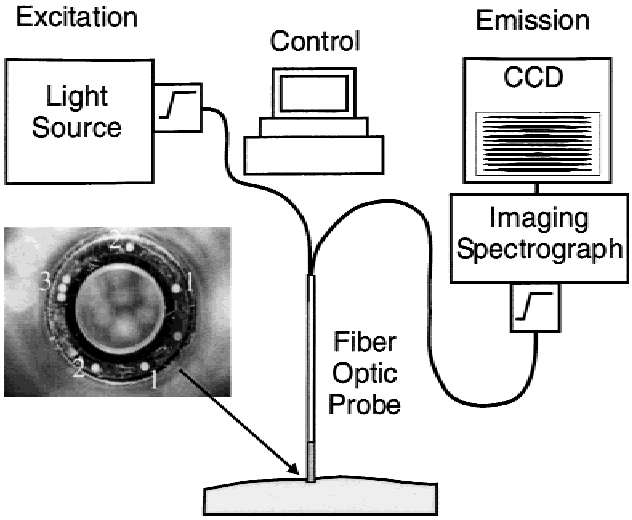

Fig. 1. Block diagram of the optical spectroscopy system. Broad-band illumination is provided by a Xenon arc lamp. An optical fiber probe is placed directly in contact with the tissue, and diffuse reflectance is collected at three different source-detector separations (E = source,1,2,3 = detector).

Mourant et al. [17] used reflectance spectroscopy to distinguish malignant from nonmalignant sites in the bladder and found a sensitivity of 100% and a specificity of 97%. Ge et al. [18] used it to distinguish neoplastic from nonneoplastic sites in colonic tissue and reported a sensitivity of 86% and specificity of 84%. Koenig et al. [19] used reflectance spectroscopy during cystoscopy to distinguish between neoplastic and benign bladder mucosa and calculated a sensitivity of 91% and specificity of 60%. Feld [20] used reflectance spectroscopy to detect Barrett's esophagus and found as much agreement (71%) between the reflectance measurements as was found between the diagnoses of four different pathologists. Zonios et al. [21] used diffuse reflectance data from human adenomatous colon polyps to fit an analytical model and found that differences can be attributed to hemoglobin concentration and effective scatterer size.

In this study, we examine the potential of diffuse reflectance spectroscopy to detect ovarian neoplasia. We present results of an exploratory pilot study to measure reflectance spectra at three different source-detector separations from normal and neoplastic ovarian tissue in 16 women.

MATERIALS AND METHODS

Materials

A spectroscopic system (see Fig. 1 for a block diagram) was used to collect reflectance spectra from ovarian tissue in vivo. The spectroscopic system, described in detail elsewhere [29], includes (1) a Xenon arc lamp equipped with a 295-nm long-pass filter that provides broadband illumina-

tion, (2) a fiberoptic probe that directs light to the tissue and collects diffusely reflected light from three source-detector separations (positions 1, 2, and 3), and (3) an imaging spectrograph and charge-coupled device camera that detects the reflected light intensity as a function of wavelength. The probe tip is placed in contact with the tissue. Fibers for illumination and collection of diffuse reflectance are arranged in a ring at the edge of the probe. The collection fibers are located 1.1 mm (position 1), 2.1 mm (position 2), and 3 mm (position 3) from a single illumination fiber. All fibers have a core diameter of 200 μm. White light from the Xenon lamp is coupled to the proximal end of the illumination fiber. The distal ends of the fibers are flush with the probe tip and placed in direct contact with the sample surface.

By using this system, ovarian tissue reflectance spectra from 390 nm to 590 nm were collected in approximately 30 seconds. Spectral resolution was 7 nm with a sampling frequency of 2 nm. The signal-to-noise ratio exceeded 75:1 for 90% of the data. By using this same system, fluorescence emission spectra at 18 different excitation wavelengths can also be collected [29], but in this study, we present results based only on reflectance spectra.

Patients

Patients undergoing exploratory laparotomy and oophorectomy at The University of Texas M. D. Anderson Cancer Center, Hermann Hospital, and Lyndon B. Johnson (LBJ) Harris County Hospital in Houston, Texas, were asked to participate in this in vivo reflectance spectroscopy study. Informed consent was obtained from each patient who participated. The study was reviewed and approved by the Institutional Review Boards of The University of Texas at Austin, M. D. Anderson, Hermann Hospital, and LBJ Hospital. At the time of exploratory laparotomy, reflectance spectra were acquired from two to six sites, both normal and abnormal appearing, before disrupting the blood supply. Tissue biopsies were obtained from all sites after they had been identified visually and analyzed by the probe. Comments were recorded on whether the tissue appeared neoplastic or appeared grossly normal. Eighteen women enrolled in the study, and their ages ranged from 31 to 75 years with a mean age of 54 years. Two women were premenopausal, and the remainder were postmenopausal.

Pathology

At the time of laparotomy, all specimens were collected from the area that was interrogated optically and subsequently fixed in formalin. Hematoxylin and eosin staining was done in the standard manner, and slides were examined by a single gynecologic pathologist (E.G.S.) in a manner blind to the spectroscopy results. Samples were classified pathologically into eight categories based on the most prevalent pathology: normal ovary (no structures except stroma and epithelium), stromal hyperplasia (high cellularity of stroma), corpus luteum, corpus albicans, endosalpingiosis, inclusion cyst, benign neoplasm, or cancer [30] The first six categories are all normal variants in the ovary.

Data Review

All spectra were reviewed by a single investigator in a manner blind to the pathologic results (UU). Spectra were discarded if values were very low (five measurements) (indicating that the probe was not in proper contact with the tissue) or anomalies such as spikes caused by cosmic radiation were present (one measurement).

Data Processing

Reflectance spectra were wavelength calibrated with a mercury light source. Dark current and background were recorded before each measurement at the same settings but with the illumination turned off. These background measurements were subtracted off-line from each reflectance measurement. Reflectance data were reported relative to reflectance data from a 2.68% (vol) solution of 1.072 μm diameter polystyrene microspheres (Polyscience, Inc., Warrington, PA). In brief, the probe was placed on the outside wall of a 1-cm path length cuvette containing the microsphere solution. The total integrated reflectance of this standard was then measured on a double-beam spectrophotometer (U-3300 Hitachi, Tokyo, Japan) with an integrating sphere attachment (Labsphere, Inc., North Sutton, NH). This method was used to correct the reflectance measurements of the microsphere solution made with the spectroscopic system. Tissue spectra at each collection fiber position were divided pointwise by the corrected standard reflectance spectrum at the corresponding fiber position.

Reflectance spectra were further processed to reduce noise. A moving average with a width of 10 nm was applied to each spectrum; after this, intensities of all reflectance spectra were extracted in 5-nm steps from 400 nm to 585 nm and individually analyzed. In addition, the slope of the reflectance spectrum was calculated between 400 nm and 580 nm in 5-nm steps. The slope of the spectrum at each wavelength was calculated from a least-squares fit to a straight line of a 20-nm section (10 measurement points) of the spectrum centered on the wavelength of interest. In addition, the total integrated reflectance was calculated from 390 to 590 nm and from 440 to 590 nm. The integrated measurement between 440 and 590 avoids the spectral area, which is most affected by blood absorption. A diagnostic device that relies on slope measurements would not require absolute intensity calibration. The total integrated intensity is a measure of the overall brightness and is similar to a black and white picture.

For purposes of data analysis, samples were grouped in three categories on the basis of the histopathologic diagnosis: normal findings (normal stroma, stromal hyperplasia, endosalpingiosis, simple cysts, corpus luteum, and corpus albicans), benign neoplasms, and cancer. We explored methods to discriminate normal findings from benign neoplasms and cancers (which would be of interest in

TABLE 1. Summary of Pathology Data and Sites Measured

	No. of sites position 1	No. of sites position 2	No. of sites position 3	No. of patients
Total sites	63	64	60	16
Normal	51	51	48	14
Cyst	3	3	3	3
Endosalpingiosis	7	7	7	3
Corpus luteum	2	2	2	1
Corpus albicans	8	8	8	6
Hyperplasia	15	15	14	8
Normal with no other structures	16	16	14	7
Benign tumor	6	6	5	3
Cancer	6	7	7	4

the screening setting) and benign neoplasms from cancers (which would be of interest in the diagnostic setting).

Analysis

For each diagnostic category (normal, benign neoplasm, cancer), we calculated the average value and standard deviation of the intensity at each wavelength, the slope at each wavelength, and the integrated intensity from 390 to 590 nm and from 440 to 590 nm. These values were calculated separately for each source detector separation. Student's *t*-test was used to determine where differences between the mean values for all three categories were statistically largest.

Although spectra were measured from multiple sites within each patient, each observation was treated independently. Visual inspection of the spectra indicated that differences between spectra from different normal sites within a patient were approximately the same as differences between spectra from normal sites in different patients, supporting our assumption that interpatient variability for the same pathologic diagnosis was minimal. The same was found for spectra from sites with cancer.

We used two approaches to identify promising optical parameters. The sum of *P* values by using the Student's *t*-test was calculated for the following tissue category combinations:

$$\text{Screening sum} = p(\overline{OP}_\lambda(\text{normal}) \text{ vs. } \overline{OP}_\lambda(\text{benign neoplasm})) + p(\overline{OP}_\lambda(\text{normal}) \text{ vs. } \overline{OP}_\lambda(\text{cancer}))$$

$$\text{Diagnosis sum} = p(\overline{OP}_\lambda(\text{normal}) \text{ vs. } \overline{OP}_\lambda(\text{benign neoplasm})) + p(\overline{OP}_\lambda(\text{normal}) \text{ vs. } \overline{OP}_\lambda(\text{cancer})) + p(\overline{OP}_\lambda(\text{benign neoplasm}) \text{ vs. } \overline{OP}_\lambda(\text{cancer}))$$

where $\overline{OP}_\lambda$ indicates the mean value of an optical parameter at a particular wavelength.

The first sum was used to assess how mean optical parameters of normal tissue differed from those of benign neoplasms and cancers. The second sum was used to assess how mean optical parameters differed among all three categories.

Because a statistical difference in the means of two categories does not necessarily suggest the ability to accurately discriminate between them, a combination of the most promising parameters was further investigated with threshold classifiers. Parameters that were examined further for their diagnostic ability were the ones that produced the lowest sums of *P* values. We constructed two-dimensional scatterplots for each site measured, to determine how well these parameters could effectively discriminate between the three categories of normal, benign neoplasm and cancer.

To test whether the differences initially found are truly correlated with the diagnosis or arise from fluctuations in the random noise, the analysis procedure was repeated under the following conditions: We randomly assigned sample diagnosis 5,000 times while preserving the original disease prevalence. For each random assignment, we examined the *P* value for each optical property as a function of wavelength. Based on the random assignments we determined the level where 1% of these 5,000 trials had a smaller sum of *P* values. This level is a measure of how likely the sum of *P* values could have been achieved by chance. All calculations and graphs were produced with the Matlab® (Mathworks, Inc.) and the Statistical Toolbox for Matlab.

RESULTS

Patient Observations

Twenty patients were enrolled in our study, and we placed the probe on 76 sites. Hardware failure during the initial measurement sequence prevented measurement in 4 patients. We measured spectra from 72 sites in 16 patients. Biopsy results were not available from four measured sites. Because of software error, no reflectance data were acquired from position 3 for four sites. Visual inspection ruled out five spectra for position 1, four for position 2, and four for position 3. Spectra were rejected because four sites showed a very low signal indicating that the probe was not sufficiently in contact with the tissue, and one spectrum showed a saturation spike probably caused by cosmic radiation. After blinded review of spectra and pathology, spectra from 64 sites in 16 patients provided data that could be analyzed further. Of the two premenopausal patients, one had only normal findings and one had

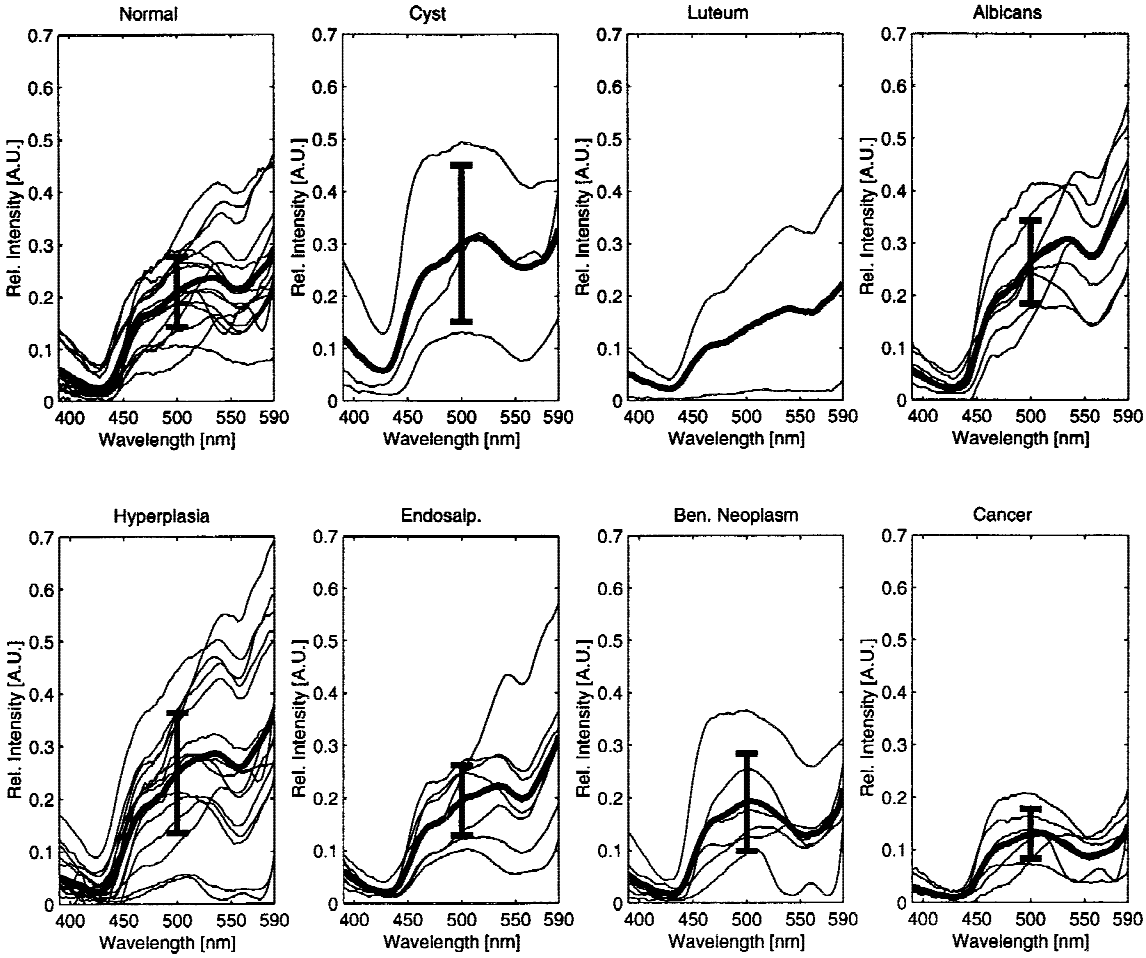

Fig. 2. Reflectance spectra at fiber position 1 for all sites, by diagnostic category (normal tissue, cyst, corpus luteum, corpus albicans, hyperplasia, endosalpingiosis, benign neoplasm, and cancer). The dark line shows the mean spectrum (± 1 standard deviation) for each category (error bars were not plotted for corpus luteum because the number of samples was two).

a benign neoplasm (cystadenoma) adjacent to normal sites. Of the 16 postmenopausal patients, 9 had only normal findings, 1 had bilateral benign neoplasms, 2 had normal sites adjacent to benign neoplasms, and 4 had cancerous sites adjacent to normal sites. Table 1 shows the number of samples with usable data measured in each of the diagnostic categories. This analysis resulted in 51 normal findings (16 normal sites with no other structures, 7 endosalpingiosis, 3 simple cysts, 2 corpus luteum, 8 corpus albicans, 15 stromal hyperplasia), 6 benign neoplasms, and 7 cancers.

Reflectance Spectra

Figure 2 shows reflectance spectra from all sites measured for fiber position 1, grouped according to eight diagnostic categories. Average spectra are also shown for each diagnostic category, with error bars corresponding to the standard deviation at 500 nm. Figure 3 shows average spectra for each diagnostic category on the same graph. At

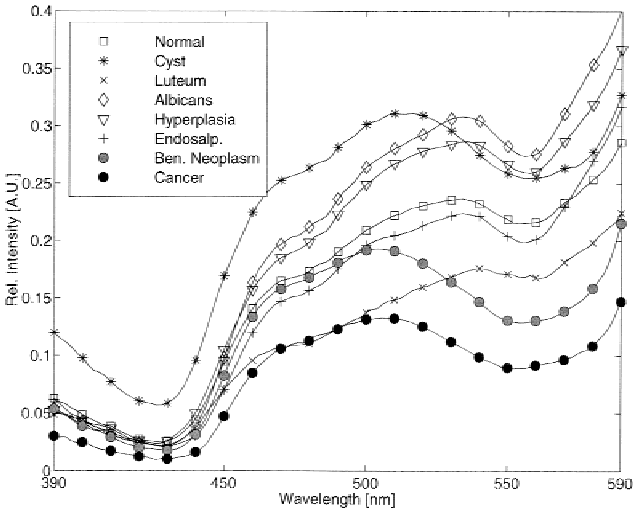

Fig. 3. Mean reflectance spectra at fiber position 1 for all eight diagnostic categories.

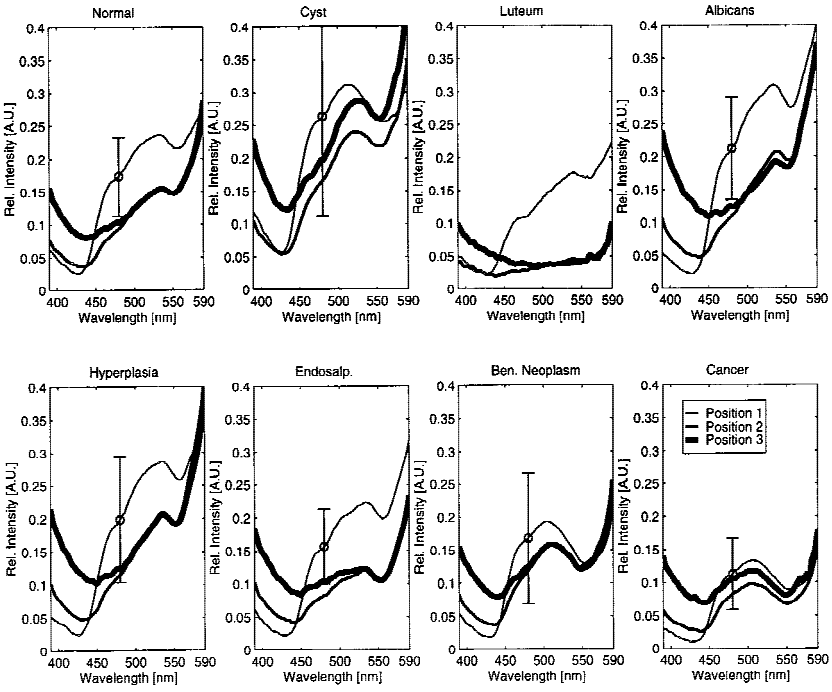

Fig. 4. Mean reflectance spectra at each fiber position for all eight diagnostic categories. The line width increases from fiber position 1 to position 3. Standard deviation is plotted for fiber position 1. Standard deviation for positions 2 and 3 were similar.

all wavelengths, cancer sites had the lowest average reflected intensity, whereas simple cysts, corpus albicans, and stromal hyperplasia had the highest reflected intensity. At wavelengths longer than 500 nm, differences in the intensity of reflected light between normal tissues, benign neoplasms, and cancers were the greatest. In addition, the slope of the average reflectance spectra from 500 to 520 nm differed between normal tissues and benign neoplasms and cancers. In this range, the slope of the average reflectance spectra was positive for normal tissue but negative for both benign neoplasms and cancers.

Figure 4 shows the mean spectra obtained at fiber positions 1, 2, and 3 for all eight diagnostic categories. Error bars show the standard deviation at 480 nm for position 1 (standard deviation was approximately the same for all positions).

Figure 5 shows the screening sum, i.e., the sum of the P values comparing the mean intensity and mean slopes of normal tissue versus benign neoplasms and normal tissue versus cancers, at each wavelength at the three different source-detector separations. A low value indicated a statistically large difference of the parameters; we were particularly interested in those with values less than 0.1. The largest statistical differences in mean intensity were found at approximately 580 nm at all fiber positions, although the intensity differences in fiber position 1 were the largest, statistically. At all fiber positions, the slope at approximately 520 nm showed the largest statistical difference.

Table 2 lists the eight intensities and slopes at each fiber position corresponding to the lowest sum of the P values. This analysis was repeated for the diagnosis sum, i.e., the sum of the P values for normal tissues versus benign neoplasms, normal tissue versus cancers, and benign neoplasms versus cancers. At all positions, intensities in the range of 535–585 nm and slopes in the region of 495–535 nm were ranked as most different. From Table 2, we selected the parameter that showed the largest statistical differences for each fiber position and each method of comparison. The mean value and standard deviation of these parameters for each of the eight diagnostic categories are shown in Figures 6 and 7. Parameters based on the integrated intensity were not promising in this analysis, indicating that the overall brightness of the reflected light may not be a good diagnostic predictor. Figure 6 shows the parameter corresponding to the lowest screening sum. Figure 6A shows the mean slope at 520 nm for position 1; Figure 6B shows the mean slope at 520 nm for position 2; and Figure 6C shows the mean slope at 525 nm for position 3. In fiber position 2, the mean slope at 520 nm for cancer sites and benign neoplasms was negative, whereas for all normal conditions the slope was positive. In fiber position 1, the slope for cancer sites and benign neoplasms was more negative than in fiber position 2 but simple cysts also had a negative slope. Benign neoplasms had a slope similar to cancer sites. Similar results were obtained for the slope at 525 nm in position 3 (Fig. 6C). Corpus albicans had the highest positive mean slope at all three positions, followed by stromal hyperplasia sites at fiber positions 2 and 3.

Figure 7 shows the parameters corresponding to the lowest diagnosis sum. Figure 7A shows the mean intensity at 585 nm for position 1; Figure 7B shows the mean slope at 505 nm for position 2; and Figure 7C shows the mean slope at 510 nm for position 3. At fiber position 1, the intensity at 585 nm was lowest for cancer sites, whereas sites with corpus albicans and stromal hyperplasia had the highest reflectance intensity. At fiber position 2, the

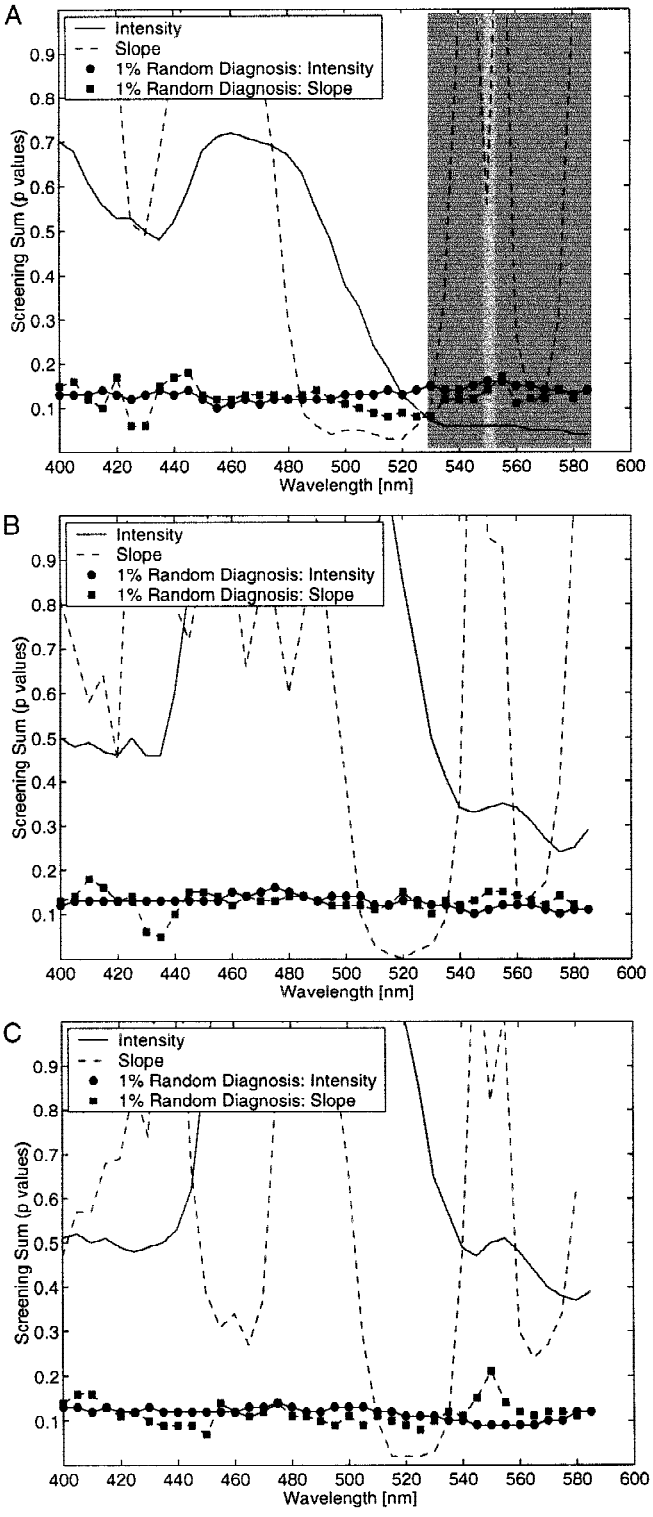

Fig. 5. Sum of *P* values for differences in the mean reflectance intensity (solid lines) and slope (dashed lines) as a function of wavelength for normal tissue versus benign tumors and normal tissue versus cancers at (**A**) fiber position 1, (**B**) fiber position 2, and (**C**) fiber position 3. Shaded areas indicate areas where the sum of *P* values is below 0.1. Also plotted (circles, squares) is the level where 1% of 5,000 trials with randomly assigned diagnosis has a lower sum of *P* values.

mean slope at 505 nm was lowest for cancer tissue. The mean slopes at 505 nm were also low for corpus luteum, benign neoplasms, and endosalpingiosis at fiber position 2. For fiber position 3, the mean slope at 510 nm was negative for cancers and positive for all other tissue categories. The mean slopes at 510 nm were close to zero for benign neoplasms, corpus luteum, and endosalpingiosis at fiber position 3.

When the data were analyzed in this way by using the randomly assigned diagnosis, statistical differences were not found. When the sum of the *P* values found with the correct diagnosis was less than 0.1 (shaded areas of Fig. 5), it was also less than the sum found for more than 99% of the 5,000 trials run with the random diagnosis. This finding indicates that the wavelength regions identified as most promising for screening and diagnostic ability by using the true diagnosis were very likely not due to correlations with random noise in the spectral data. However, Figures 6 and 7 also show that the mean values for the normal, benign and neoplastic groups are not separated by values larger than 1 standard deviation, indicating the need to combine several parameters to create a discriminatory variable.

Discrimination of Normal, Benign, and Malignant Tissues

To determine whether these differences would enable separation of all samples into the categories of normal ovary, benign neoplasms, and ovarian cancers, two-dimensional scatterplots were generated, combining the value of two promising optical parameters for each site measured. Parameters in this analysis were selected from Figure 5, which showed that for separation of normal tissues from benign neoplasms and cancers, the most promising parameters were the intensity from 530 to 580 nm at position 1, the slope from 490 to 520 nm at position 1, the slope from 510 to 530 nm at position 2, and the slope from 510 to 530 nm at position 3. These regions are indicated by the shaded gray areas in Figure 5. Two-dimensional scatterplots containing all possible pairwise combinations of these four groups of parameters at 10-nm intervals were then generated (96 total combinations). Figure 8 shows a representative example, plotting the slope at 495 nm vs. the intensity at 585 nm at position 1 for all 63 sites measured at fiber position 1.

The straight line labeled *screening* represents a threshold classifier for separating normal ovarian findings from benign neoplasms and cancers. The line was drawn to minimize the total number of sites misclassified. Fourteen normal sites and 1 cancer site were misclassified, resulting in a training set sensitivity of 92% (11 of 12) and a specificity of 73% (37 of 51). This process was repeated for all pairwise combinations of these parameters, resulting in an average sensitivity of 86 ± 6% and an average specificity of 79 ± 5%.

The straight line labeled *diagnostic* represents an algorithm for separating normal ovarian tissue and benign neoplasms from cancers. The line was drawn to minimize

TABLE 2. Optical Parameters With the Largest Statistical Differences Between Normal Tissue (N), Benign Tumors (B), and Cancers (C)*

Position 1				Position 2				Position 3			
N-B, N-C, B-C		N-B, N-C		N-B, N-C, B-C		N-B, N-C		N-B, N-C, B-C		N-B, N-C	
I 585	0.20	S 520	0.03	S 505	0.30	S 520	0.00	S 510	0.52	S 525	0.02
I 580	0.28	S 515	0.03	I 575	0.37	S 515	0.01	S 570	0.57	S 520	0.02
I 565	0.32	S 510	0.04	I 580	0.38	S 525	0.02	S 505	0.61	S 515	0.02
I 575	0.33	S 495	0.04	I 570	0.38	S 530	0.03	S 575	0.63	S 530	0.03
I 560	0.33	I 585	0.04	I 585	0.39	S 510	0.03	S 535	0.64	S 535	0.10
I 555	0.33	I 580	0.04	I 565	0.39	S 535	0.09	I 580	0.65	S 510	0.10
I 535	0.33	S 505	0.05	I 560	0.41	S 505	0.10	I 575	0.65	S 565	0.24
I 570	0.34	S 500	0.05	I 555	0.41	S 565	0.14	S 515	0.66	S 570	0.27

*Tabulated are the smallest sums of *P* values corresponding to differences in the mean slop (S) or the intensity (I) at different wavelengths and fiber positions.

the total number of sites misclassified. Six normal sites, one benign site, and one cancer site were misclassified, resulting in a sensitivity of 83% (5 of 6) and a specificity of 88% (50 of 57). This process was repeated for all pairwise combinations of these parameters, resulting in an average sensitivity of 86 ± 4% and an average specificity of 80 ± 8%.The histopathology of all misclassified sites was reviewed a second time in an attempt to understand the cause of their misclassification. The cancer that was misclassified as a benign neoplasm had no tumor on the surface but had microscopic islands of tumor cells in the stroma.

DISCUSSION

The results presented here show that both slope and intensity of reflectance spectra may have the ability to discriminate normal from abnormal conditions of the ovary. Slopes between 510 nm and 530 nm were most promising at all investigated source-detector separations. Intensities between 530 nm and 585 nm with a short source-detector separation of 1.1 mm also provided useful discriminatory information. A combination of two parameters of either slope or intensity detected abnormal conditions with an average sensitivity of 86 ± 6% and an average specificity of 79 ± 5%.

Several groups have found promising results in clinical trials of reflectance spectroscopy for detection of neoplasia. Mourant et al. [17] hypothesized that the differences detected with their system between 330 and 370 nm were caused by the influence of scattering, which is affected by the nuclear-to-cytoplasmic ratio [25], whereas Koenig et al. [19] and similarly Zonios et al. [21] concluded that total blood concentration was the most promising optical parameter. The algorithm developed by Ge et al. [18] also favored intensities at the absorption peaks of oxy- and deoxyhemoglobin.

Our findings in ovarian tissue compare well with the findings of these four groups. Like Koenigs's and Ge's groups, we found that intensities between 550 and 580 nm, which are strongly affected by blood absorption, are an indicator of neoplastic associated changes in the ovary. At the location of an isosbestic point of oxy- and deoxyhemoglobin absorption, the slope of the reflectance spectrum changes most dramatically with blood oxygenation. We also found that *P* values were largest for slopes between 510 and 530 nm, a range that lies very close to an isosbestic point at 500 nm. The slight offset to the actual maxima of the isosbestic point indicates that scattering may also contribute to the separation of ovarian tissue conditions.

In recent years, endoscopic evaluation of the peritoneal cavity has been instituted in those patients wishing to have a laparoscopic procedure done in the office under local anesthesia. A 3-mm endoscope is inserted into the peritoneal cavity and a small amount of pneumoperitoneum is created to allow visualization of the pelvic organs [31]. The development of office laparoscopy in combination with quantitative optical spectroscopy may provide a less expensive and safer method of investigating abnormalities identified by TVS, because it does not require general anesthesia and uses a much smaller probe. To integrate these findings into a screening device, imaging modalities that can be performed endoscopically need to be investigated. Reflectance images can be measured with bandpass-filtered cameras. The slope of the reflectance spectrum can be determined with two images measured with slightly wavelength-shifted bandpass filters. An imaging system based on the same parameters presented in Figure 8 would require three measurements. Bandpass filtering can be easily accomplished through an endoscope. Our findings indicate that a system equipped with a filter at 580 ± 10 nm and two filters at 525 ± 10 nm and 505 ± 10 nm to measure the slope at 520 nm is most promising.

Based on this exploratory study, we have shown that reflectance spectroscopy may have the capability to identify differences between normal structures and cancer and the potential to provide minimally invasive diagnostic imaging in near real time. However, we plan to conduct further trials with sufficient sample size to increase the power of these conclusions and to verify the results. A larger sample size will allow us to use more sophisticated statistical methods with mixed models by using analysis

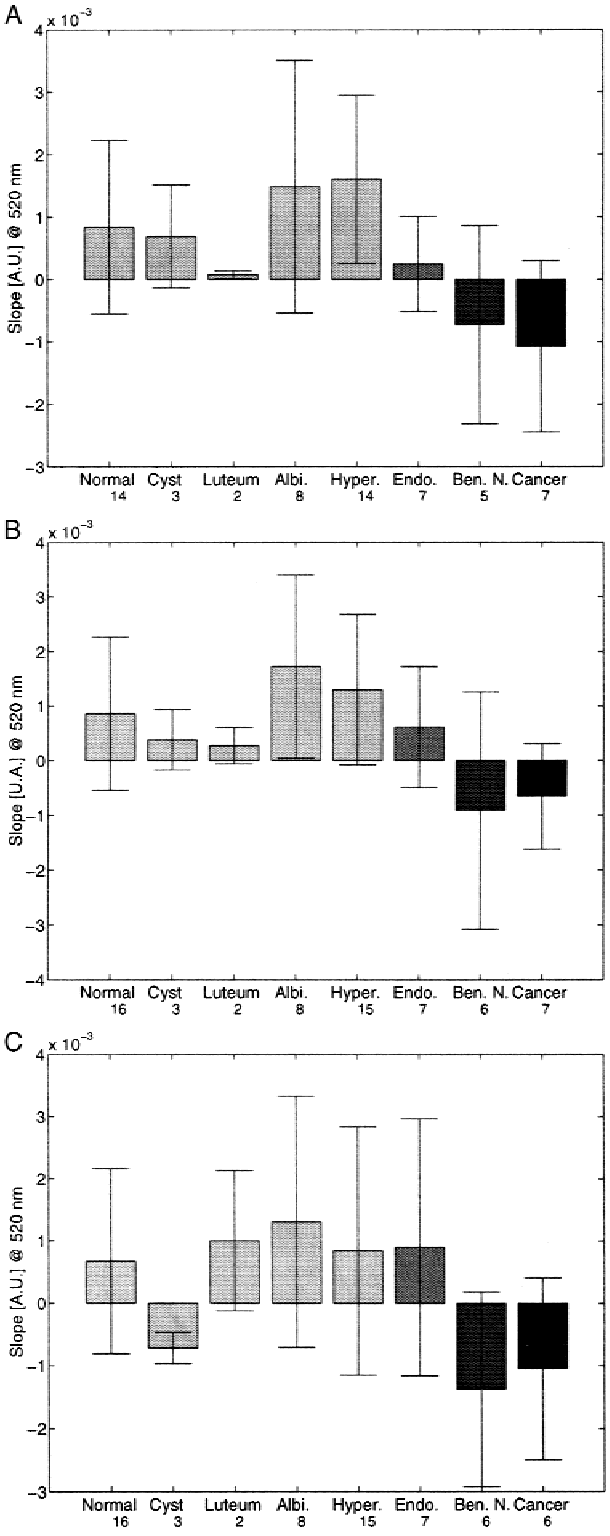

Fig. 6. Parameters corresponding to the largest statistical differences in mean reflectance spectra of normal tissue versus benign tumors and normal tissue vs. cancers. Parameters are shown separately for the three different source-detector separations: (**A**) fiber position 1, slope at 520 nm; (**B**) fiber position 2, slope at 520 nm; (**C**) fiber position 3, slope at 520 nm.

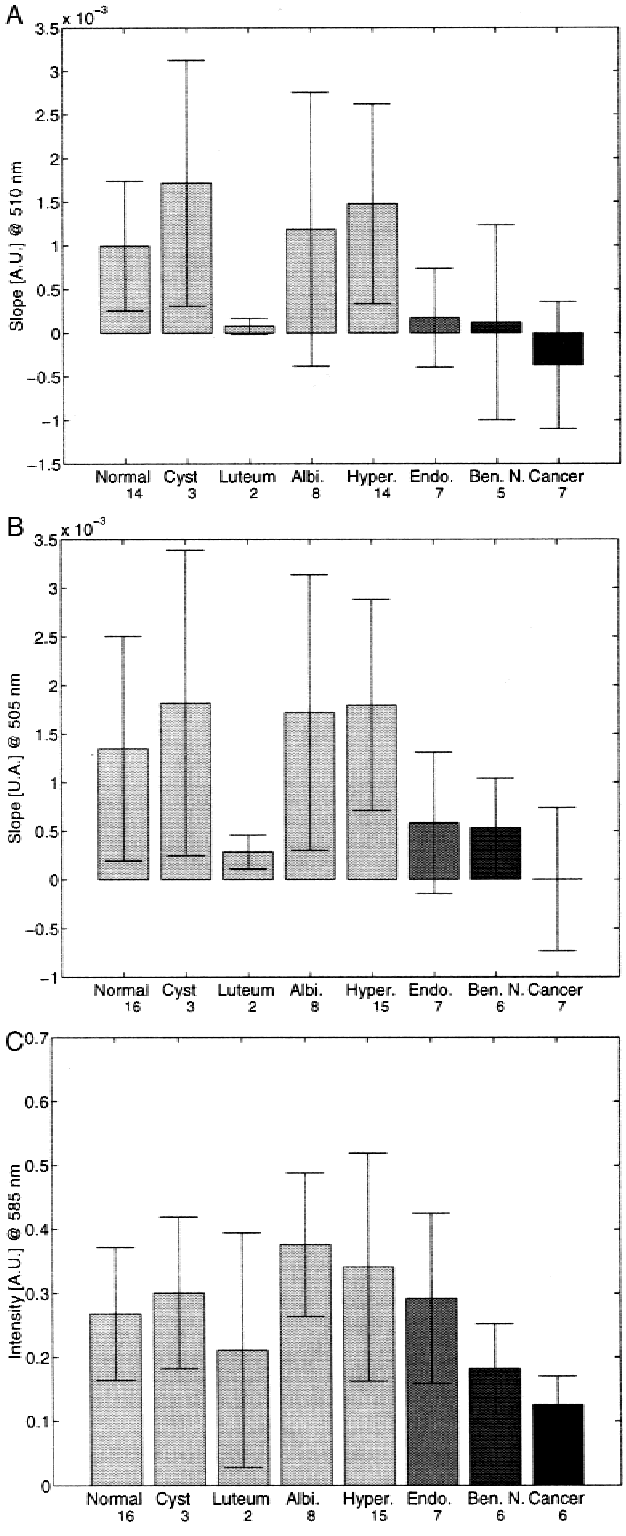

Fig. 7. Parameters corresponding to largest statistical differences in mean reflectance spectra of normal tissue versus benign tumors, normal tissue versus cancers, and benign neoplasms versus cancers. Parameters are shown separately for the three different source detector separations: (**A**) fiber position 1, intensity at 585 nm; (**B**) fiber position 2, slope at 505 nm; (**C**) fiber position 3, slope at 510 nm.

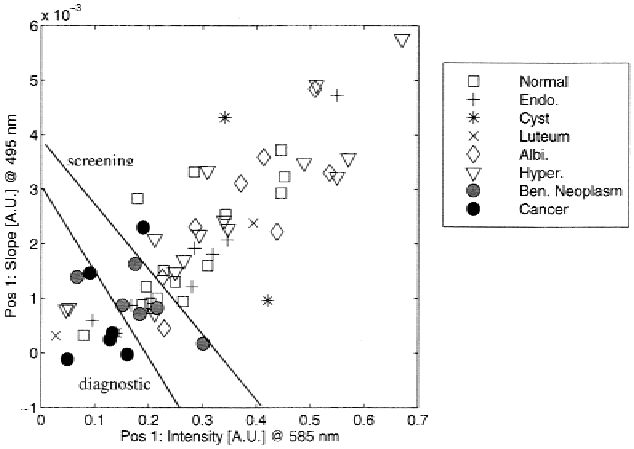

Fig. 8. Two-dimensional scatterplot showing the slope at 495 nm vs. the intensity at 585 nm at position 1 for each of the 63 sites measured. Endo., endosalpingiosis; Albi., corpus albicans; Hyper., hyperplasia; Ben., benign.

of variance with replicates and logistic regression. Power calculations will be based on the data accrued in this pilot study.

To date, early diagnosis and screening of ovarian cancer have been hampered by the intraperitoneal location of the ovaries, which has necessitated a surgical procedure to assess the ovaries directly. Serum markers in series or in parallel with ultrasound can only evaluate the ovaries indirectly. Spectroscopy is a methodology that is adaptable to use in office laparoscopy or with a transvaginal probe to access the ovaries which deserves further study based on the results of this small pilot trial.

ACKNOWLEDGMENTS

We gratefully acknowledge funding from the Texas Higher Education Coordinating Board, the Swiss Foundation for Medical and Biological Scholarships and Dennis Cox for the helpful discussions.

REFERENCES

1. American Cancer Society. www.cancer.org.
2. Wingo PA, Tong T, Bolden S. Cancer statistics. Ca Cancer J Clin 1995;45:8–30.
3. Hoskins WJ. Prospective on ovarian cancer: Why prevent? J Cell Biochem Suppl 1995;23:189–199.
4. de Bruijn HW, van der Zee AG, Aalders JG. The value of cancer antigen 125 (CA 125) during treatment and follow-up of patients with ovarian cancer. Curr Opin Obstet Gynecol 1997;9:8–13.
5. Berek JS, Bast RC Jr. Ovarian cancer screening: the use of serial complementary tumor markers to improve sensitivity and specificity for early detection. Cancer 1995;76:2092–2096.
6. Karlan BY. The status of ultrasound and color Doppler imaging for the early detection of ovarian carcinoma. Cancer Invest 1997;15:265–269.
7. NIH Consensus Development Panel on Ovarian Cancer: Ovarian cancer screening, treatment and follow-up. JAMA 1995;273:491–497.
8. Zurawski VR, Orjaseter H, Andersen A, Jellum E. Elevated serum CA 125 levels prior to diagnosis of ovarian neoplasia: Relevance for early detection of ovarian cancer. Int J Cancer 1988;42:677–680.
9. Vuento MH, Stenman UH, Pirhonen JP, Makinen JI, Laippala PJ, Salmi TA. Significance of a single CA 125 assay combined with ultrasound in the early detection of ovarian and endometrial cancer. Gynecol Oncol 1997;64:141–147.
10. Miki Y, Swensen JJ, Shattuck-Eidens D, Futreal PA, Harshman K, Tavtigian S, Liu Q, Cochran C, Bennett LM, Ding W, et al. A strong candidate for the breast and ovarian cancer susceptibility gene BRCA1. Science 1994;266:66–71.
11. Rhei E, Bogomolniy F, Federici MG, Maresco DL, Offit K, Robson ME, Saigo PE, Boyd J. Molecular genetic characterization of BRCA1- and BRCA2-linked hereditary ovarian cancers. Cancer Res 1998;58:3193–3196.
12. Lerman C, Narod S, Schulman K, Hughes C, Gomez-Caminero A, Bonney G, Gold K, Trock B, Main D, Lynch J, Fulmore C, Snyder C, Lemon SJ, Conway T, Tonin P, Lenoir G, Lynch H. BRCA1 testing in families with hereditary breast-ovarian cancer: a prospective study of patient decision making and outcomes. JAMA 1996;275:1885–1892.
13. Mackey SE, Creasman WT: Ovarian cancer screening. J Clin Oncol 1995;13:783–793.
14. DePriest PD, van Nagell JR Jr, Gallion HH, Shenson D, Hunter JE, Andrews SJ, Powell DE, Pavlik EJ. Ovarian cancer screening in asymptomatic postmenopausal women. Gynecol Oncol 1993;51:205–209.
15. Van Nagell JR Jr, DePriest PD, Puls LE, Donaldson ES, Gallion HH, Pavlik EJ, Powell DE, Kryscio RJ. Ovarian cancer screening in asymptomatic postmenopausal women by transvaginal sonography. Cancer 1991;68:458–462.
16. Runowitz C. Advances in the screening and treatment of ovarian cancer. CA Cancer J Clin 1992;42:327–349.
17. Mourant JR, Bigio IJ, Boyer J, Conn RL, Johnson T, Shimada T. Spectroscopic diagnosis of bladder cancer with elastic light scattering. Lasers Surg Med 1995;17:350–357.
18. Ge Z, Schomacker KT, Nishioka NS: Identification of colonic dysplasia and neoplasia by diffuse reflectance spectroscopy and pattern recognition techniques. Appl Spectrosc 1998;52: 833–345.
19. Koenig F, Larne R, Enquist H, McGovern FJ, Schomacker KT, Kollias N, Deutsch TF. Spectroscopic measurement of diffuse reflectance for enhanced detection of bladder carcinoma. Urology 1998;51:342–345.
20. Feld MS: Spectral pathology using reflected light. In: Biomedical optical spectroscopy and diagnostics, technical digest. Optical Society of America, Washington DC: 2/BMA1-1, 1998.
21. Zonios G, Perelman LT, Backman V, Manahoran R, Fitzmaurice M, Van Dam J, Feld MS. Diffuse reflectance spectroscopy of human adenomatous colon polyps in vivo. Appl Optics 1999;38:6628–6637.
22. Bigio IJ, Mourant JR: Ultraviolet and visible spectroscopies for tissue diagnostics: fluorescence spectroscopy and elastic-scattering spectroscopy. Phys Med Biol 1997;42:803–814.
23. Richards-Kortum R, Sevick-Muraca E. Quantitative optical spectroscopy for tissue diagnosis. Annu Rev Phys Chem 1996;47:555–606.
24. Mahadevan-Jansen A, Richards-Kortum R. Raman spectroscopy for the detection of cancers and precancers. J Biomed Optics 1996;1:31–70.
25. Perelman LT, Backman V, Wallace M, Zonios G, Nanoharan R, Nusrat A, Shields S, Seiler M, Lima C, Hamano T, Itzkan I, Van Dam J, Crawford JM, Feld MS. Observation of periodic fine structure in reflectance from biological tissue: a new technique for measuring nuclear size distribution. Physl Rev Lett 1998;80:627.
26. Dunn AK, Smithpeter CL, Welch AJ, Richards-Kortum R. Sources of contrast in confocal reflectance imaging. Appl Optics 1996;35:3441–3447.

27. Mourant JR, Freyer JP, Hielscher AH, Eick AA, Shen A, Johnson TM. Mechanism of light scattering from biological cells relevant to noninvasive optical-tissue diagnostics. Appl Optics 1998;37:3586–3593.
28. Zijlstra WG, Buursma A, Meeuwsen-van der Roest WP. Absorption spectra of human fetal and adult oxyhemoglobin, de-oxyhemoglobin, carboxyhemoglobin, and methemoglobin. Clin Chem 1991;37:1633–1638.
29. Zuluaga AF, Utzinger U, Durkin A, Fuchs H, Gillenwater A, Jacob R, Kemp B, Fan J, Richards-Kortum R: Fluorescence excitation emission matrices of human tissue: a system for in vivo measurement and method of data analysis. Appl Spectrosc 1998;53:301–311.
30. Kurman RJ: Blaustein's pathology of the female genital tract. New York: Springer-Verlag;1994.
31. Runowicz CD. Office laparoscopy as a screening tool for early detection of ovarian cancer. J Cell Biochem Suppl 1995;23: 238–242.